SUBMITTED TO *The Astrophysical Journal*
Preprint typeset using LaTeX style emulateapj v. 08/13/06

ESTIMATING BLACK HOLE MASSES IN ACTIVE GALACTIC NUCLEI USING THE Mg II λ2800 EMISSION LINE

JIAN-GUO WANG[1,2,5,6], XIAO-BO DONG[2,4], TING-GUI WANG[2,4], LUIS C. HO[3], WEIMIN YUAN[1], HUIYUAN WANG[2,4], KAI ZHANG[2,4], SHAOHUA ZHANG[2,4], AND HONGYAN ZHOU[2,4]

Submitted to The Astrophysical Journal

ABSTRACT

We investigate the relationship between the linewidths of broad Mg II λ2800 and Hβ in active galactic nuclei (AGNs) to refine them as tools to estimate black hole (BH) masses. We perform a detailed spectral analysis of a large sample of AGNs at intermediate redshifts selected from the Sloan Digital Sky Survey, along with a smaller sample of archival ultraviolet spectra for nearby sources monitored with reverberation mapping. Careful attention is devoted to accurate spectral decomposition, especially in the treatment of narrow-line blending and Fe II contamination. We show that, contrary to popular belief, the velocity width of Mg II tends to be smaller than that of Hβ, suggesting that the two species are not cospatial in the broad-line region. Using these findings and recently updated BH mass measurements from reverberation mapping, we present a new calibration of the empirical prescriptions for estimating virial BH masses for AGNs using the broad Mg II and Hβ lines. We show that the BH masses derived from our new formalisms show subtle but important differences compared to some of the mass estimators currently used in the literature.

Subject headings: black hole physics — galaxies: active — quasars: emission lines — quasars: general

1. INTRODUCTION

It is generally accepted that active galactic nuclei (AGNs) are powered by the release of gravitational energy from material accreted onto supermassive black holes (BHs). The determination of BH mass ($M_{\rm BH}$) is crucial for understanding the AGN phenomena, the cosmological evolution of BHs, and even the coevolution of AGNs and their host galaxies. Yet, for such distant objects, it is currently impossible to obtain direct measurement of $M_{\rm BH}$ using spatially resolved stellar or gas kinematics. Fortunately, significant advances have been made in recent years from reverberation mapping (RM) studies of nearby Seyfert galaxies and QSOs (e.g., Wandel et al. 1999; Kaspi et al. 2000; Peterson et al. 2004). First, the correlation between the radius of the broad-line region (BLR) and the velocity width of broad emission lines supports the idea that the BLR gas is virialized and that its velocity field is dominated by the gravity of the BH (Peterson & Wandel 1999, 2000; Onken & Peterson 2002). Second, the size of the BLR scales with the continuum luminosity (Kaspi et al. 2000, 2005), approximately as $R \propto L^{0.5}$ (Bentz et al. 2006, 2009); the $R-L$ relation offers a highly efficient procedure for estimating the BLR size without carrying out time-consuming RM observations. And third, the BH masses estimated by RM are roughly consistent (Gebhardt et al. 2000b; Ferrarese et al. 2001; Nelson et al. 2004; Onken et al. 2004) with the predictions from the tight correlation between $M_{\rm BH}$ and bulge stellar velocity dispersion established for inactive galaxies (the $M_{\rm BH}$–$\sigma_\star$ relation; Gebhardt et al. 2000a; Ferrarese & Merritt 2000). These developments imply that we can estimate the BH mass in type 1 (broad-line, unobscured) AGNs by simple application of the virial theorem, $M_{\rm BH} = fRv^2/G$, where f is a geometric factor of order unity that depends on the geometry and kinematics of the line-emitting region, R is the radius of the BLR derived from the AGN luminosity, and v is some measure of the virial velocity of the gas measured from single-epoch spectra. The feasibility of obtaining R and v from single-epoch spectra enables $M_{\rm BH}$ to be estimated very efficiently for large samples of AGNs, especially for luminous quasars at higher redshift that typically exhibit only slow and small-amplitude variability (e.g., Kaspi et al. 2007). In practice, for those AGNs that have measurements of $\sigma_\star$, f is determined empirically by scaling the virial masses to the $M_{\rm BH}$–$\sigma_\star$ relation of inactive galaxies (e.g., Onken et al. 2004). Implicit in this practice is the assumption — one open to debate (Greene & Ho 2006; Ho et al. 2008; Kim et al. 2008) — that active and inactive BHs should follow the same $M_{\rm BH}$–$\sigma_\star$ relation. The most widely used estimator for v is the full-width at half maximum (FWHM) of the line.

Now, a large number of formalisms to estimate $M_{\rm BH}$ from single-epoch spectra have been proposed in the recent literature, using different broad emission lines optimized for different redshift regimes probed by (widely available) optical spectroscopy. At low redshifts, the lines of choice are Hβ (Kaspi et al. 2000; Collin et al. 2006; Vestergaard & Peterson 2006) or Hα (Greene & Ho 2005); at intermediate redshifts, Mg II λ2800 is used (McLure & Jarvis 2002); while at high redshifts, one has to resort to C IV λ1549 (Vestergaard 2002; Vestergaard & Peterson 2006). These formalisms are ultimately calibrated against RM masses based on the Hβ BLR radius and linewidth measured from the variable (rms) spectra (Peterson et al. 2004). Because the Hβ linewidth is typically smaller in the rms spectra than in the single-epoch or mean spectra (Vestergaard 2002; Collin et al. 2006; Sulentic et al. 2006), some authors have proposed that the FWHM used in the Hβ-based formalisms should be further corrected to obtain unbiased $M_{\rm BH}$ estimates (Collin et al. 2006; Sulentic et al. 2006).

[1] National Astronomical Observatories/Yunnan Observatory, Chinese Academy of Sciences, P.O. Box 110, Kunming, Yunnan 650011, China; wangjg, wmy@ynao.ac.cn
[2] Key Laboratory for Research in Galaxies and Cosmology, The University of Sciences and Technology of China, Chinese Academy of Sciences, Hefei, Anhui 230026, China; xbdong, twang@ustc.edu.cn
[3] The Observatories of the Carnegie Institution of Washington, 813 Santa Barbara Street, Pasadena, CA 91101, USA; lho@ociw.edu
[4] Center for Astrophysics, University of Science and Technology of China, Hefei, Anhui 230026, China
[5] Department of Physics, Yunnan University, Kunming, Yunnan 650031, China
[6] Graduate School of the Chinese Academy of Sciences, 19A Yuquan Road, P.O. Box 3908, Beijing 100039, China

As for the Mg II-based formalisms, because there are very few RM experiments of the Mg II line, they are either based on the RM data for Hβ (e.g., McLure & Jarvis 2002; McLure & Dunlop 2004) or calibrated against the Hβ formalisms themselves (e.g., Kollmeier et al. 2006; Salviander et al. 2007). A strong, underlying assumption is that Mg II and Hβ are emitted from the same location in the BLR and have the same linewidth (see also Onken & Kollmeier 2008). In support of this assumption, some authors find that Mg II and Hβ indeed have very similar linewidths (e.g., McLure & Jarvis 2002; McLure & Dunlop 2004; also cf. Salviander et al. 2007). However, there are conflicting results in the literature: Corbett et al. (2003) claim that Mg II is generally broader than Hβ, whereas Dietrich & Hamann (2004) come to an opposite conclusion. Certainly, the most direct way to settle this issue is through direct RM of the Mg II line. So far there are only two objects that have successful Mg II RM, NGC 5548 (Clavel et al. 1991; Dietrich & Kollatschny 1995) and NGC 4151 (Metzroth et al. 2006). These studies tentatively suggest that Mg II responds more slowly to continuum variations than Hβ, implying that the Mg II-emitting region is larger than that radiating Hβ.

Thus, there are still some important open questions regarding the robustness of $M_{\rm BH}$ measurements based on Mg II. What is the relation between the linewidths of Hβ and Mg II? Are estimates of $M_{\rm BH}$ based on Mg II consistent with those based on Hβ? These basic questions are critical for understanding the systematic uncertainties in studies of the cosmological evolution of BHs (cf. Shen et al. 2008; McGill et al. 2008; Denney et al. 2009a). To address the above questions, we perform a detailed comparison of the widths of the Mg II and Hβ lines using single-epoch spectra for a large, homogeneous sample of Seyfert 1 nuclei and QSOs at intermediate redshifts culled from the Sloan Digital Sky Survey (SDSS; York et al. 2000). We further compare single-epoch Mg II linewidths with Hβ linewidths measured from the rms spectra of AGNs with RM observations, finding systematic deviations between the two. We present a recalibration of the Mg II virial mass estimator and compare our formalism with previous ones in the literature.

This paper adopts the following set of cosmological parameters: H_0=70 km s^{-1} Mpc^{-1}, Ω_m=0.3, and Ω_Λ=0.7.

2. SAMPLE AND DATA ANALYSIS

2.1. *The Samples*

The sample of best-studied Hβ emission lines is the one compiled by Peterson et al. (2004) for RM studies of 35 low-redshift AGNs. To compare Hβ and Mg II for this sample, we located usable ultraviolet (UV) spectra for 29 sources, 16 from the *Hubble Space Telescope (HST)* and 13 from the *International Ultraviolet Explorer (IUE)* data archives. This sample will be used to study the relationship between single-epoch Mg II linewidths and Hβ linewidths measured from rms spectra, and to fit a new $M_{\rm BH}$ formalism based on single-epoch Mg II.

We also selected Seyfert 1 galaxies and QSOs in the redshift range $0.45 < z < 0.75$ from the Fifth Data Release (DR5) of the SDSS spectroscopic database (Adelman-McCarthy et al. 2007). Within this redshift range, both Hβ and Mg II lie within the SDSS spectral coverage. To ensure accurate measurement of both lines, we only select objects with a mean signal-to-noise ratio (S/N) $\geq$ 20 per pixel in both the Hβ (4600–5100 Å) and the Mg II (2700–2900 Å) regions. Our final SDSS sample contains 495 objects. This sample will be used to investigate the FWHM relation between Mg II and Hβ in single-epoch spectra and to compare our Mg II formalism with others in the literature.

2.2. *Spectral Fitting*

The spectra are first corrected for Galactic extinction using the extinction map of Schlegel et al. (1998) and the reddening curve of Fitzpatrick (1999).

To measure the Hβ line, we perform continuum subtraction and emission-line fitting following the method described in detail in Dong et al. (2008). We first fit simultaneously the featureless nonstellar continuum (assumed to be a power law), the Fe II multiplet emission, and other emission lines in the wavelength range 4200–5600 Å, giving emphasis on the proper determination of the local pseudocontinuum (continuum + Fe II emission). For spectra with fits having a reduced $\chi^2 > 1.1$ around Hβ (4750–5050 Å), a refined fit of the emission-line profiles is performed to the pseudocontinuum-subtracted spectra using the code described in Dong et al. (2005). Each line of the [O III] $\lambda\lambda$4959,5007 doublet is modeled with two Gaussians, one accounting for the line core and the other for a possible blue wing as seen in many objects. The doublet lines are assumed to have the same redshifts and profiles, and the flux ratio λ5007/λ4959 is fixed to the theoretical value of 3. The narrow component of Hβ is fitted with one Gaussian, assumed to have the same width as the line core of [O III] λ5007. The broad component of Hβ is fitted with as many Gaussians as statistically justified (see Dong et al. 2008 for details).

To measure the Mg II line, a power-law local continuum, a Balmer continuum, and an Fe II emission template, which together constitute the so-called pseudocontinuum, are first fitted simultaneously. The fitting is performed in the restframe wavelength range 2200–3500 Å, with the small region contaminated significantly by Mg II masked out. The fitting range is set by the wavelength coverage of the UV Fe II template, which was generated by Tsuzuki et al. (2006) based on their measurements of I Zw 1. In the wavelength region covered by Mg II emission, they employed a semi-empirical iteration procedure to build the template. They first generated a theoretical Fe II model spectrum with the photoionization code CLOUDY (Ferland et al. 1998) and subtracted it from the observed I Zw 1 spectrum around Mg II. Then the Mg II doublet was fit assuming each line has the same profile as Hα. And finally they obtained the Fe II template underneath Mg II by subtracting the Mg II fit from the observed spectrum.

The model for the nonstellar featureless continuum is a simple power law,

$$f^{\rm PL}(\lambda) = a\left(\frac{\lambda}{2200}\right)^{\beta} \quad . \tag{1}$$

As in Dietrich et al. (2002), the Balmer continuum is assumed to be produced in partially optically thick clouds with a uniform temperature, [7]

[7] We do not account for the velocity broadening of the Balmer continuum, because the Balmer continuum in our fitting range is insensitive to this effect.

$$f^{\rm BaC}(\lambda) = cB_\lambda(\lambda, T_e)(1-e^{-\tau_\lambda}); \quad \lambda \leq \lambda_{\rm BE} \tag{2}$$

$$\tau_\lambda = \tau_{\rm BE}\left(\frac{\lambda}{\lambda_{\rm BE}}\right)^3, \tag{3}$$

where $\lambda_{\rm BE} = 3646$ Å (3.4 eV), $\tau_{\rm BE}$ is the optical depth at $\lambda_{\rm BE}$, and $B_\lambda(\lambda, T_e)$ is the Planck blackbody spectrum at the electron temperature T_e. During the fitting, the parameters a and β of the power-law continuum, the parameters c, T_e, and $\tau_{\rm BE}$ of the Balmer continuum, and the normalization, velocity broadening, and velocity shift of the Fe II template are set to be free parameters.

We note that in the fitting range of 2200–3500 Å the Balmer continuum is hard to be constrained and separated from the power-law continuum and Fe II emission (cf. Figure 8 of Tsuzuki et al. 2006). In this work we are not concerned with the properties of the Balmer continuum, but with the proper separation of the power-law continuum, Fe II, and Mg II. To minimize the effect of the possible poor fitting of Balmer continuum on the determination of the power-law continuum, Fe II, and Mg II, in practice we adopt the following procedure:

1. To obtain reasonable parameters for the featureless continuum, we first fit the power-law continuum alone using several continuum windows near 2200, 3000, 4000, and 4200 Å that suffer little from emission-line contamination.

2. We then fit the 2200–3500 Å region using the above three-component model, with the power-law continuum parameters constrained to vary only around the best-fit values obtained from the first step, by a factor of $<10\%$ for the normalization a and $< 20\%$ for the slope β. During this step, we assign additionally larger weights to the regions 2400–2650 Å and 2920–2990 Å in order to improve the fit for the Fe II emission surrounding Mg II (cf. Section 2.3 of Dong et al. 2008).

Once the pseudocontinuum is fitted and subtracted, each of the two Mg II $\lambda\lambda$2796, 2803 doublet lines is modeled with two components, one broad and one narrow. The broad component is a truncated five-parameter Gauss-Hermite series (van der Marel & Franx 1993; see also Salviander et al. 2007); the narrow component is a single Gaussian. The broad components of the doublet lines are set to have the same profile, with the flux ratio λ2796/λ2803 set to be between 2:1 and 1:1 (Laor et al. 1997), and the doublet separation set to the laboratory value. The same prescription is applied to the narrow components, with the following additional constraints: FWHM ≤ 900 km s^{-1} and flux $< 10\%$ of the total Mg II flux (Wills et al. 1993; see also McLure & Dunlop 2004).

There are several other emission lines in the fitting region, identified from the composite SDSS QSO spectrum (see Table 2 of Vanden Berk et al. 2001); yet, because of their weakness, we simply masked them out in the fit. Because of the limited wavelength coverage of the RM sample, we cannot separate the Balmer continuum from the power-law continuum. Thus, the Balmer continuum was not included in the fits for this sample. Additionally, there are deep narrow absorption features around Mg II in the spectra of NGC 3227, NGC 3516, NGC 3783, and NGC 4151 in the RM sample. Each of the absorption features is fitted simultaneously with a Gaussian when fitting the Mg II emission line.

We estimate the measurement uncertainties of the parameters using the bootstrap method described in Dong et al. (2008, Section 2.5). The estimated 1 σ errors for the broad-line fluxes are typically 10% for Mg II and 8% for Hβ, while the errors on the broad-line FWHM are $\sim$20% for Mg II and $\sim$15% for Hβ. The power-law continua have uncertainties of 8% for the slope and 5% for the normalization.

Figure 1 shows two examples of the fits. The continuum and emission-line parameters for the RM and SDSS samples are listed in Tables 1 and 2, respectively. The data and fitting parameters are available online for the decomposed spectral components (continuum, Fe II, and other emission lines). [8]

2.3. *Regression Methods*

In the next section, we will fit the data using several regression methods. The purpose of using these different methods is for ease of comparison with results in the literature, and to investigate possible differences in the fitting results caused by the different methods. Here we briefly summarize the regression methods used.

1. Ordinary least-squares (OLS) without considering measurement errors.

2. Weighted least-squares (WLS) that takes into account only measurement uncertainties in the dependent variable.

3. FITexy (Press et al. 1992) is a variant of orthogonal-distance regression, and accounts for measurement uncertainties in both coordinates.

4. FITexy_T02, the version of FITexy modified by Tremaine et al. (2002), accounts for possible intrinsic scatter in the dependent variable by adding in quadrature a constant to the error value so as to obtain a reduced χ^2 of 1.

5. Gaussfit (McArthur et al. 1994) is a robust least-squares estimator that can handle errors in both coordinates.

6. The bivariate correlated errors and intrinsic scatter (BCES) regression method (Akritas & Bershady 1996), using both the bisector and orthogonal versions.

7. LINMIX_ERR (Kelly 2007) is a Bayesian approach that can account for measurement errors, censoring, and intrinsic scatter. We also consider the multivariate extension, MLINMIX_ERR.

3. RESULTS

The main motivation of this work is to investigate whether reliable BH masses can be estimated using the Mg II linewidth as a virial velocity indicator. Linewidths are commonly parameterized as either FWHM or $\sigma_{\rm line}$, the line dispersion or second moment of the line profile. Both quantities have intrinsic strengths and weaknesses (see Section 3 of Peterson et al. 2004). Collin et al. (2006), in particular, argue that the use of FWHM rather than $\sigma_{\rm line}$ introduces systematic bias in $M_{\rm BH}$ estimates. However, the line dispersion is very sensitive to measurement errors in the line wings, making it especially susceptible to inaccuracies caused by deblending and

[8] Available at http://staff.ustc.edu.cn/~xbdong/Data_Release/MgII_Hbeta/, together with auxiliary code to explain the parameters and to demonstrate the fitting.

subtraction of Fe II and other emission lines, effects that are particularly significant in mean and single-epoch spectra. By contrast, the FWHM is less prone to these effects; it is more sensitive to corrections for the narrow-line component, which, fortunately, is quite weak for Mg II (see Section 4.1). In this work we opt to use the FWHM to parameterize the linewidth.

3.1. *Single-epoch Mg II FWHM vs. Hβ FWHM*

We first investigate the relation between the FWHM of Mg II and Hβ, using single-epoch data from our SDSS sample. The relation is illustrated in Figure 2. A strong correlation is present, but apparently deviates from one-to-one. This trend has been noticed in the literature, but it was less prominent because of the narrower dynamical range in velocity covered in previous studies (e.g., Salviander et al. 2007; Hu et al. 2008). With our high-quality data, we can now fit a strict relation. We perform a linear regression in log-log space using the methods described in Section 2.3; the results are listed in Table 2. For our subsequent analysis, we adopt the BCES(orthogonal) method because it treats both variables symmetrically. We find

$$\log\left[\frac{\mathrm{FWHM(Mg\,II)}}{1000\ \mathrm{km\ s^{-1}}}\right] = (0.81\pm0.02)\log\left[\frac{\mathrm{FWHM(H\beta)}}{1000\ \mathrm{km\ s^{-1}}}\right] + (0.05\pm0.01). \quad (4)$$

This means that *the line-emitting locations of Hβ and Mg II in the BLR are not identical*.

3.2. *Single-epoch Mg II FWHM vs. rms Hβ $\sigma_{\rm line}$*

Since the assumption that Mg II FWHM is identical to Hβ FWHM does not hold, we explore the relation between Mg II FWHM and rms Hβ $\sigma_{\rm line}$, which has been argued to be a good tracer of the virial velocity of the BLR clouds emitting (variable) Hβ (see references in Section 1). We use data for the 29 objects in the RM sample that have UV spectra to perform this exploration. Mg II FWHM is measured from the single-epoch *HST/IUE* spectra, as listed in Table 1. The data for rms Hβ $\sigma_{\rm line}$ are mainly taken from Peterson et al. (2004). In addition, we use updated RM data for NGC 4051 (Denney et al. 2009b), NGC 4151 (Metzroth et al. 2006), NGC 4593 (Denney et al. 2006), NGC 5548 (Bentz et al. 2007), and PG 2130+099 (Grier et al. 2008). For objects with multiple measurements, the geometric mean (i.e. the mean in log scale) was used.

We find that the slope of the relation between Mg II FWHM and rms Hβ $\sigma_{\rm line}$ deviates from unity, with a best fit of

$$\log\left[\frac{\sigma_{\rm line}(\mathrm{H\beta,rms})}{1000\ \mathrm{km\ s^{-1}}}\right] = (0.85\pm0.21)\log\left[\frac{\mathrm{FWHM(Mg\,II)}}{1000\ \mathrm{km\ s^{-1}}}\right] - (0.21\pm0.12)\ . \quad (5)$$

Such a nonlinear relation between Mg II FWHM and rms Hβ $\sigma_{\rm line}$ is not very surprising, in light of a similar situation observed for Hβ FWHM (Collin et al. 2006; also Sulentic et al. 2006, Section 1). For verification, we also fit the relation between Hβ FWHM in the mean spectra and rms Hβ $\sigma_{\rm line}$ using data for 35 objects in the RM sample; the FWHM data are taken from Collin et al. (2006) and from the updated sources mentioned above. The best-fit relation deviates from unity even more seriously than the case of Mg II FWHM:

$$\log\left[\frac{\sigma_{\rm line}(\mathrm{H\beta,rms})}{1000\ \mathrm{km\ s^{-1}}}\right] = (0.54\pm0.08)\log\left[\frac{\mathrm{FWHM(H\beta,mean)}}{1000\ \mathrm{km\ s^{-1}}}\right] - (0.09\pm0.05)\ . \quad (6)$$

These relations between Mg II and Hβ FWHM and rms Hβ $\sigma_{\rm line}$ are illustrated in Figure 3.

3.3. *Practical Formalism for New Mg II-based $M_{\rm BH}$ Estimator*

As described above, Mg II FWHM is not identical to, but rather generally smaller than, Hβ FWHM; for Mg II FWHM $\gtrsim 6000$ km s^{-1}, the difference is $\gtrsim 0.2$ dex. This means that one of the fundamental premises of the previous Mg II-based formalisms — that Mg II and Hβ trace similar kinematics — does not hold. Moreover, similar to the behavior of Hβ FWHM, Mg II FWHM seems not to be linearly proportional to rms Hβ $\sigma_{\rm line}$. If rms $\sigma_{\rm line}$ is more directly linked to the virial velocity, this implies that we cannot build a virial $M_{\rm BH}$ formalism by simply assuming $M_{\rm BH} \propto \mathrm{FWHM}^2$. Furthermore, the $M_{\rm BH}$ data of the RM AGNs used in McLure & Jarvis (2002) and McLure & Dunlop (2004) have since been recalibrated or updated (Peterson et al. 2004; Denney et al. 2006, 2009b; Metzroth et al. 2006; Bentz et al. 2007; Grier et al. 2008). Thus, it is necessary to reformulate the virial $M_{\rm BH}$ formalism based on single-epoch Mg II FWHM.

We proceed by assuming that there is a tight relation between the BLR radius of the Mg II-emitting region and the AGN continuum luminosity, in the form $R_{\rm Mg\,II} \propto L^{\beta}$, and another between the virial velocity of Mg II and the FWHM of the line, in the form $v^2_{\rm virial} \propto \mathrm{FWHM}^{\gamma}$. Then, using the $M_{\rm BH}$ data for the RM sample (Table 1), we calculate the free parameters by fitting

$$\log\left[\frac{M_{\rm BH}(\mathrm{RM})}{10^6\,M_\odot}\right] = a+\beta\log\left(\frac{L_{3000}}{10^{44}\ \mathrm{erg\ s^{-1}}}\right) + \gamma\log\left[\frac{\mathrm{FWHM(Mg\,II)}}{1000\ \mathrm{km\ s^{-1}}}\right]\ , \quad (7)$$

where $L_{3000} \equiv \lambda L_\lambda(3000\ \text{Å})$. The RM-based $M_{\rm BH}$ data are mainly taken from Peterson et al. (2004), who calibrated the f-factor by normalizing to the $M_{\rm BH}$–σ_* relation of Onken et al. (2004); $M_{\rm BH}$ for the updated objects comes from the references given in Section 3.2.

We fit Equation (7) following four schemes, using the (LINMIX_ERR/MLINMIX_ERR) method of Kelly (2007):

1. a, β, and γ are treated as free parameters.
2. a and β are treated as free parameters, but, as in all previous formalisms, we fix $\gamma = 2$.
3. a and β are treated as free parameters, but we set $\gamma = 1.70$, as suggested by Equation (5).
4. a and γ are treated as free parameters, but we fix $\beta = 0.5$, as suggested by the latest $R-L$ relation (Bentz et al. 2006, 2009).

Table 4 lists the best-fit regression for each scheme (Cols. 1–4), as well as comparisons between the $M_{\rm BH}$ estimates therefrom and the RM-based masses (Col. 5). It is apparent that the best-fit values for β for all the schemes are consistent with 0.5 within a $1\,\sigma$ error. Interestingly, γ appears to be

marginally smaller than 2, since the standard deviation of the BH mass for Scheme 2 is slightly larger than that for the other three schemes. If we set $\beta = 0.5$ (i.e. adopt Scheme 4), the best-fit Mg II-based formalism is

$$\log\left(\frac{M_{\rm BH}}{10^6 M_\odot}\right) = (1.13 \pm 0.27) + 0.5 \log\left(\frac{L_{3000}}{10^{44}\ {\rm erg\ s^{-1}}}\right) + (1.51 \pm 0.49) \log\left[\frac{\rm FWHM(Mg\,II)}{1000\ {\rm km\ s^{-1}}}\right] \quad (8)$$

Fitting the Hβ FWHM data for the 35 RM objects under the same assumptions ($\beta = 0.5$), the Hβ-based formalism becomes

$$\log\left(\frac{M_{\rm BH}}{10^6 M_\odot}\right) = (1.39 \pm 0.14) + 0.5 \log\left(\frac{L_{5100}}{10^{44}\ {\rm erg\ s^{-1}}}\right) + (1.09 \pm 0.23) \log\left[\frac{\rm FWHM(H\beta)}{1000\ {\rm km\ s^{-1}}}\right] \quad (9)$$

The best-fitting $\gamma = 1.09 \pm 0.23$ agrees well with the $\sigma_{\rm line}({\rm H}\beta, {\rm rms}) - {\rm FWHM(H}\beta)$ relation derived in Equation (6).

Our new $M_{\rm BH}$ formalisms using Mg II FWHM (Equation 8) and Hβ FWHM (Equation 9) are illustrated in Figure 4.

Figure 5 compares our new Mg II-based formalism (we show only Schemes 2 and 4) with the previous Hβ-based formalisms of Vestergaard & Peterson (2006; *panel a*) and Collin et al. (2006; *panel b*), as well as our newly derived version using the SDSS sample of 495 Seyfert 1s and QSOs (Equation 9; *panel c*). The $M_{\rm BH}$ residuals between our Mg II formalism and the Hβ formalisms are listed in Table 4 (Cols. 6–8). While our Mg II-based formalism, especially for Scheme 4 (Eqn. 8), agrees well with our Hβ-based formalism (Eqn. 9), note that it deviates markedly from the Hβ formalism of Vestergaard & Peterson. This confirms previous suspicions (Collin et al. 2006; Sulentic et al. 2006) that the use of Hβ FWHM from mean and single-epoch spectra with the assumption $\gamma = 2$ introduces systematic bias into $M_{\rm BH}$ estimates.

We further compare our new Mg II-based formalism (Eqn. 8) with other Mg II formalisms widely used in the literature. Figure 5 illustrates that the $M_{\rm BH}$ estimates following the formalisms of McLure & Dunlop (2004; *panel d*), Kollmeier et al. (2006; *panel e*), and Salviander et al. (2007; *panel f*) show large systematic deviations, mostly in the sense of being smaller than ours. The deviations stem primarily from the recalibration of the RM masses; other factors are discussed in Section 4.3. We note that a yet-unpublished Mg II-based formalism by M. Vestergaard et al. (in preparation) used in the recent literature (e.g., Kelly et al. 2009) is almost identical to our Scheme 2 (with γ fixed to 2).

4. DISCUSSION

4.1. *Testing the Effect of Narrow-line Subtraction*

The narrow component of Mg II is generally weak in luminous type 1 AGNs (e.g., Wills et al. 1993; Laor et al. 1994), and so its contribution to the total line flux can be safely neglected. However, its presence might have a more pronounced impact on the FWHM measurement of broad Mg II. In the literature, narrow Mg II was accounted for in the line fitting by some authors (e.g., McLure & Dunlop 2004), but not by others (e.g., Salviander et al. 2007). As there is usually no clear inflection in the Mg II profile, separating narrow Mg II from the broad component is often challenging. Fortunately, for the spectra in our SDSS sample, [O III] λ5007 is present, and thus we can use [O III] to try to constrain narrow Mg II, to test the effect of narrow Mg II on the FWHM measurement of broad Mg II, and also to test the reliability of our Mg II fitting strategy.

In addition to the default fitting strategy described in Section 2.2, in which narrow Mg II is modeled as a single free Gaussian, we tried two alternative strategies in which narrow Mg II is (A) not fit at all, and (B) is fit using a single-Gaussian model constrained to that of the line core of [O III]. Broad Mg II is modeled as described in Section 2.2. We find that, for the 495 objects in our SDSS sample, the distributions of the reduced χ^2 of the three approaches can be approximated reasonably well with a log-normal function. The peak and standard deviation of the reduced χ^2 are very similar for all three, being (0.97, 0.10 dex) for the default strategy, (1.01, 0.10 dex) for Strategy A, and (0.99, 0.10 dex) for Strategy B. Regarding the FWHM of broad Mg II, the mean and standard deviation are (–0.04, 0.05) for $\log[\frac{\rm FWHM(A)}{\rm FWHM(default)}]$ and (0.00, 0.05) for $\log[\frac{\rm FWHM(B)}{\rm FWHM(default)}]$. For Strategy B, the fitted flux of narrow Mg II is less than 10% of the total line flux for almost all the objects. Our tests show that omitting the subtraction of narrow Mg II has a negligible effect on the FWHM of broad Mg II, typically decreasing it only by a tiny factor of 0.04 dex. We further confirm that our default procedure for modeling narrow Mg II is consistent with that using the [O III] core as a template.

The above Strategy A is exactly the same as the Mg II-fitting method adopted by Salviander et al. (2007). We also compared our method with that of McLure & Dunlop (2004). When fitting the spectra in our SDSS sample by the method of McLure & Dunlop (2004), on average the FWHM of broad Mg II is larger than that of our method by 0.1 dex.

4.2. *$M_{\rm BH}$ Estimators with Single-epoch Hβ and Mg II*

As analyzed in detail by Sulentic et al. (2006), the overall profile of the Hβ emission line, as viewed in single-epoch spectra, likely comprises multiple components emitted from different sites. First, as a recombination line, Hβ can arise from BLR gas that is very close to the central engine. Then Hβ can be gravitationally redshifted, as (part of) the component of the "very broad-line region" (Marziani & Sulentic 1993). Such clouds may be optically thin to the ionizing continuum, such that Hβ is no longer responsive to continuum variation (Shields et al. 1995). Second, like C IV λ1549, Hβ can be produced partly in high-ionization winds, as some observations suggest (see Marziani et al. 2008 and references therein). This wind component would not be virial. Third, Hβ can also be produced on the surface of the accretion disk, both by recombination and collisional excitation (Chen & Halpern 1989; Wang et al. 2005; Wu et al. 2008); this component would be highly anisotropic (cf. Collin et al. 2006). Considering the above factors, it is not surprising that single-epoch FWHM is not linearly proportional to $\sigma_{\rm line}$ for rms Hβ (Eqn. 6).

Mg II, as a low-ionization, collisionally excited emission line, cannot be produced in clouds very close to the central engine. Furthermore, because Mg II originates only from optically thick clouds, radiation pressure force cannot act on them very significantly (cf. Marconi et al. 2008, 2009; Dong et al. 2009), and thus Mg II suffers little from nonvirial motion. Hence, compared to Hβ, the FWHM of single-epoch Mg II should, in principle, deviate less, if at all, from the true

virial velocity of the line-emitting clouds. This is suggested by the best-fit value for γ in Equation (8), which indicates $v^2_{\rm virial} \propto {\rm FWHM(Mg\,II)}^{1.51\pm0.49}$.

Previously, researchers have feared that the substantial contamination of the Mg II region by Fe II multiplets might introduce significant uncertainties in its linewidth measurements, such that Mg II-based $M_{\rm BH}$ estimates may not be as accurate as those based on Hβ. With the recent availability of a more refined UV Fe II template (Tsuzuki et al. 2006; cf. Vestergaard & Wilkes 2001), we have higher confidence that the linewidth measurements of Mg II are reasonably robust. Our work suggests that we can measure Mg II FWHM typically to within an uncertainty of $\sim$20%. Nevertheless, it would be highly desirable to attempt to further improve the methodology for Fe II subtraction, not only in the UV but also at optical wavelengths.

4.3. *Comparison with Previous Studies*

As shown in Section 3 (see Figure 5), our Mg II- and Hβ-based $M_{\rm BH}$ formalisms show subtle but systematic deviations from some of the commonly used $M_{\rm BH}$ estimators in the literature. In general, the formalism prescribed by our Scheme 4 (Eqn. 8; $M_{\rm BH} \propto {\rm FWHM}^{1.51\pm0.49}$) gives progressively higher and lower $M_{\rm BH}$ values toward the low- and high-mass ends, respectively. The only exception is the Hβ-based formalism of Collin et al. (2006), which gives roughly consistent results as ours over a relatively large mass range.

The discrepancies between previous mass estimators and ours arise from one, or a combination, of the following factors incorporated into our analysis: (1) we use the most recently updated RM BH mass measurements; (2) our new formalism (Scheme 4, Eqn. 8) uses the best-fitting value of γ instead of the canonical value of $\gamma = 2$; and (3) for Mg II, we determine the scaling factor (incorporated into the coefficient a of Eqn. 7) and the power-law index (β) of the $R_{\rm Mg\,II} - L$ relation by fitting Eqn. 7 to the data, instead of simply using the existing $R_{\rm H\beta} - L$ relation as a surrogate. Specifically, assuming the canonical value of $\gamma = 2$ in Eqn. 7 would, compared to our Scheme 4, underestimate $M_{\rm BH}$ at the low-end and overestimate $M_{\rm BH}$ at the high-end, for both Mg II and Hβ. This accounts for most of the deviations from Vestergaard & Peterson (2006) and Kollmeier et al. (2006), and partially from others in Figure 5. In order to account for systematic biases with respect to RM-based $M_{\rm BH}$, Collin et al. (2006) introduced a correction factor, which is dependent on Hβ FWHM, into their Hβ-based formalism assuming $\gamma = 2$. This correction has a similar effect as fitting γ as a free parameter, as we do here, and thus the rough consistency between our results and theirs is not surprising. Factor (3) is also partially responsible for producing the deviations from some of the previous Mg II-based $M_{\rm BH}$ estimators, such as those of McLure & Dunlop (2004) and Salviander et al. (2007), who assumed that both Mg II and Hβ obey the same $R - L$ relation, and of Kollmeier et al. (2006), who used a very steep relation of $R_{\rm Mg\,II} \propto L^{0.88}$.

There have been previous reports of discrepancies between Mg II- and Hβ-based estimators, which are sometimes claimed to correlate with luminosity or Eddington ratio (e.g., Kollmeier et al. 2006; Onken & Kollmeier 2008). These effects can be traced, at least partially, to the one-to-one relation assumed between FWHM(Mg II) and FWHM(Hβ), which is contradictory to the nonlinear relation found in this work. In fact, by adopting a nonlinear FWHM(Mg II)–FWHM(Hβ) relation and $R_{\rm Mg\,II} \propto L^{0.5}$, our new Mg II- and H$\beta$-based estimators yield mutually consistent results for the SDSS sample (Figure 5, *panel c*). We verified that the previously claimed correlations of the residuals of the Mg II- and Hβ-based estimators with luminosity or Eddington ratio largely vanish; a Spearman rank analysis indicates a chance probability of 0.09 for the former and 0.05 for the latter.

It is generally accepted that the width of the variable part of the line, the line dispersion $\sigma_{\rm line}$ measured in the rms spectrum, is by far the best tracer of the virial velocity of the BLR gas (e.g., Onken & Peterson 2002). From the virial theorem, we expect $M_{\rm BH} \propto \sigma^2_{\rm line}$. If the virial velocity is estimated using FWHM (or any other measure of the linewidth) in single-epoch spectra, as long as its relation with $\sigma_{\rm line}$ is nonlinear, γ in Eqn. 7 is expected to deviate from $\gamma = 2$. This is exactly what we find in this work for FWHM(Mg II), as well as for FWHM(Hβ). In fact, the fitted value of $\gamma = 1.51 \pm 0.49$ for Mg II (Eqn. 8) and 1.09 ± 0.23 for Hβ (Eqn. 9) are almost identical to those derived from the fitted $\sigma_{\rm line}$–FWHM(Mg II) and $\sigma_{\rm line}$–FWHM(Hβ) relations, which have slopes of 1.70 ± 0.42 and 1.08 ± 0.16, respectively. Factor (3) is justified by the compelling evidence presented in this work that the line-emitting locations of Hβ and Mg II in the BLR are not identical. Possible physical processes underlying factors (2) and (3) are discussed in Section 4.2.

Finally, the appropriateness of our approach is further justified by the fact that our formalisms give $M_{\rm BH}$ values consistent with the RM measurements with the least systematic bias. Moreover, we find consistent masses between the Mg II- and Hβ-based estimators. We thus conclude that our $M_{\rm BH}$ estimators introduce less systematic bias compared to previous formalisms. Obviously, more RM measurements (for both Hβ and Mg II) are needed in order to improve the determination of the $\sigma_{\rm line}$–FWHM relation, the $R - L$ relation, and the index γ in the $M_{\rm BH} \propto {\rm FWHM}^{\gamma}$ relation.

5. SUMMARY AND CONCLUSIONS

We investigate the relation between the velocity widths for the broad Mg II and Hβ emission lines, derived from FWHM measurements of single-epoch spectra from a homogeneous sample of 495 SDSS Seyfert 1s and QSOs at $0.45 < z < 0.75$. Careful attention is devoted to accurate spectral decomposition, especially in the treatment of narrow-line blending and Fe II contamination. We find that Mg II FWHM is systematic smaller than Hβ FWHM, as ${\rm FWHM(Mg\,II)} \propto {\rm FWHM(H\beta)}^{0.81\pm0.02}$. Using 29 AGNs that have optical reverberation-mapping data and usable archival UV spectra, we then investigate the relation between single-epoch Mg II FWHM and rms Hβ $\sigma_{\rm line}$ (line dispersion), a quantity regarded as a good tracer of the virial velocity of the BLR clouds emitting the variable Hβ component. We find that, similar to the situation for the FWHM of single-epoch Hβ, single-epoch Mg II FWHM is unlikely to be linearly proportional to rms Hβ $\sigma_{\rm line}$. The above two findings suggest that a major assumption of previous Mg II-based virial BH mass formalisms — that the Mg II-emitting region is identical to that of Hβ — is problematic. This finding and the recent updates of the reverberation-mapped BH masses (Peterson et al. 2004; Denney et al. 2006, 2009b; Metzroth et al. 2006; Bentz et al. 2007; Grier et al. 2008) motivated us to recalibrate the $M_{\rm BH}$ estimator based on single-epoch Mg II spectra.

Starting with the empirically well-motivated BLR radius-luminosity relation and the virial theorem, $M_{\rm BH} \propto L^{\beta}{\rm FWHM}^{\gamma}$. We fit the reverberation-mapped objects in a variety of different ways to constrain β and

γ. For all the strategies we have considered, β has a well-defined value of $\sim$0.5, in excellent agreement with the latest BLR radius-luminosity relation (Bentz et al. 2006, 2009), whereas $\gamma \approx 1.5 \pm 0.5$, which is marginally in conflict with the canonical value of $\gamma = 2$ normally assumed in past studies. Performing a similar exercise for Hβ yields $M_{\rm BH} \propto L^{0.5}{\rm FWHM(H}\beta)^{1.09\pm0.22}$, which again significantly departs from the functional forms used in the literature.

We use the SDSS database to compare our new $M_{\rm BH}$ estimators with various existing formalisms based on single-epoch Hβ and Mg II spectra. BH masses derived from our Mg II-based mass estimator show subtle but important deviations from many of the commonly used $M_{\rm BH}$ estimators in the literature. Most of the differences stem from the recent recalibration of masses derived from reverberation mapping. Researchers should exercise caution in selecting the most up-to-date $M_{\rm BH}$ estimators, which are presented here.

This work is supported by Chinese NSF grants NSF-10533050 and NSF-10703006, National Basic Research Program of China (973 Program 2009CB824800) and a CAS Knowledge Innovation Program (Grant No. KJCX2-YW-T05). The research of L.C.H. is supported by the Carnegie Institution of Washington. Funding for the SDSS and SDSS-II has been provided by the Alfred P. Sloan Foundation, the Participating Institutions, the National Science Foundation, the U.S. Department of Energy, the National Aeronautics and Space Administration, the Japanese Monbukagakusho, the Max Planck Society, and the Higher Education Funding Council for England. The SDSS Web Site is http://www.sdss.org/.

REFERENCES

Adelman-McCarthy, J. K., et al. 2007, ApJS, 172, 634
Akritas, M. G., & Bershady, M. A. 1996, ApJ, 470, 706
Bentz, M. C., Peterson, B. M., Pogge, R. W., Vestergaard, M., & Onken, C. A. 2006, ApJ, 644, 133
Bentz, M. C., et al. 2007, ApJ, 662, 205
Bentz, M. C., Peterson, B. M., Netzer, H., Pogge, R. W., & Vestergaard, M. 2009, ApJ, 697, 160
Chen, K., & Halpern, J. P. 1989, ApJ, 344, 115
Clavel, J., et al. 1991, ApJ, 366, 64
Collin, S., Kawaguchi, T., Peterson, B. M., & Vestergaard, M. 2006, A&A, 456, 75
Corbett, E. A., et al. 2003, MNRAS, 343, 705
Denney, K. D., et al. 2006, ApJ, 653, 152
Denney, K. D., Peterson, B. M., Dietrich, M., Vestergaard, M., & Bentz, M. C. 2009a, ApJ, 692, 246
Denney, K. D., et al. 2009b, ApJ, submitted (arXiv:0904.0251)
Dietrich, M., & Kollatschny, W. 1995, A&A, 303, 405
Dietrich, M., Appenzeller, I., Vestergaard, M., & Wagner, S. J. 2002, ApJ, 564, 581
Dietrich, M., & Hamann, F. 2004, ApJ, 611, 761
Dong, X.-B., Zhou, H.-Y., Wang, T.-G., Wang, J.-X., Li, C., & Zhou, Y.-Y. 2005, ApJ, 620, 629
Dong, X., Wang, T., Wang, J., Yuan, W., Zhou, H., Dai, H., & Zhang, K. 2008, MNRAS, 383, 581
Dong, X., Wang, J., Wang, T., Wang, H., Fan, X., Zhou, H., & Yuan, W. 2009, arXiv:0903.5020
Ferland, G. J., Korista, K. T., Verner, D. A., Ferguson, J. W., Kingdon, J. B., & Verner, E. M. 1998, PASP, 110, 761
Ferrarese, L., & Merritt, D. 2000, ApJ, 539, L9
Ferrarese, L., Pogge, R. W., Peterson, B. M., Merritt, D., Wandel, A., & Joseph, C. L. 2001, ApJ, 555, L79
Fitzpatrick, E. L. 1999, PASP, 111, 63
Gebhardt, K., et al. 2000a, ApJ, 539, L13
Gebhardt, K., et al. 2000b, ApJ, 543, L5
Greene, J. E., & Ho, L. C. 2005, ApJ, 630, 122
Greene, J. E., & Ho, L. C. 2006, ApJ, 641, L21
Grier, C. J., et al. 2008, ApJ, 688, 837
Ho, L. C., Darling, J., & Greene, J. E. 2008, ApJ, 681, 128
Hu, C., Wang, J.-M., Ho, L. C., Chen, Y.-M., Zhang, H.-T., Bian, W.-H., & Xue, S.-J. 2008, ApJ, 687, 78
Kaspi, S., Smith, P. S., Netzer, H., Maoz, D., Jannuzi, B. T., & Giveon, U. 2000, ApJ, 533, 631
Kaspi, S., Maoz, D., Netzer, H., Peterson, B. M., Vestergaard, M., & Jannuzi, B. T. 2005, ApJ, 629, 61
Kaspi, S., Brandt, W. N., Maoz, D., Netzer, H., Schneider, D. P., & Shemmer, O. 2007, ApJ, 659, 997
Kelly, B. C. 2007, ApJ, 665, 1489
Kelly, B. C., Vestergaard, M., & Fan, X. 2009, ApJ, 692, 1388
Kim, M., Ho, L. C., Peng, C. Y., Barth, A. J., Im, M., Martini, P., & Nelson, C. H. 2008, ApJ, 687, 767
Kollmeier, J. A., et al. 2006, ApJ, 648, 128
Laor, A., Bahcall, J. N., Jannuzi, B. T., Schneider, D. P., Green, R. F., & Hartig, G. F. 1994, ApJ, 420, 110
Laor, A., Jannuzi, B. T., Green, R. F., & Boroson, T. A. 1997, ApJ, 489, 656
Marconi, A., Axon, D. J., Maiolino, R., Nagao, T., Pastorini, G., Pietrini, P., Robinson, A., & Torricelli, G. 2008, ApJ, 678, 693
Marconi, A., Axon, D. J., Maiolino, R., Nagao, T., Pietrini, P., Risaliti, G., Robinson, A., & Torricelli, G. 2009, ApJ, 698, L103
Marziani, P., & Sulentic, J. W. 1993, ApJ, 409, 612
Marziani, P., Sulentic, J. W., & Dultzin, D. 2008, Rev. Mex. Astron. Astrophys. Conf. Ser., 32, 69
McArthur, B., Jefferys, W., & McCartney, J. 1994, BAAS, 26, 900
McGill, K. L., Woo, J.-H., Treu, T., & Malkan, M. A. 2008, ApJ, 673, 703
McLure, R. J., & Jarvis, M. J. 2002, MNRAS, 337, 109
McLure, R. J., & Dunlop, J. S. 2004, MNRAS, 352, 1390
Metzroth, K. G., Onken, C. A., & Peterson, B. M. 2006, ApJ, 647, 901
Nelson, C. H., Green, R. F., Bower, G., Gebhardt, K., & Weistrop, D. 2004, ApJ, 615, 652
Onken, C. A., & Peterson, B. M. 2002, ApJ, 572, 746
Onken, C. A., Ferrarese, L., Merritt, D., Peterson, B. M., Pogge, R. W., Vestergaard, M., & Wandel, A. 2004, ApJ, 615, 645
Onken, C. A., & Kollmeier, J. A. 2008, ApJ, 689, L13
Peterson, B. M., & Wandel, A. 1999, ApJ, 521, L95
Peterson, B. M., & Wandel, A. 2000, ApJ, 540, L13
Peterson, B. M., et al. 2004, ApJ, 613, 682
Press, W. H., Teukolsky, S. A., Vetterling, W. T., & Flannery, B. P. 1992 (Cambridge: Cambridge Univ. Press)
Salviander, S., Shields, G. A., Gebhardt, K., & Bonning, E. W. 2007, ApJ, 662, 131
Schlegel, D. J., Finkbeiner, D. P., & Davis, M. 1998, ApJ, 500, 525
Shen, Y., Greene, J. E., Strauss, M. A., Richards, G. T., & Schneider, D. P. 2008, ApJ, 680, 169
Shields, J. C., Ferland, G. J., & Peterson, B. M. 1995, ApJ, 441, 507
Shields, G. A., Gebhardt, K., Salviander, S., Wills, B. J., Xie, B., Brotherton, M. S., Yuan, J., & Dietrich, M. 2003, ApJ, 583, 124
Sulentic, J. W., Repetto, P., Stirpe, G. M., Marziani, P., Dultzin-Hacyan, D., & Calvani, M. 2006, A&A, 456, 929
Tremaine, S., et al. 2002, ApJ, 574, 740
Treu, T., Woo, J.-H., Malkan, M. A., & Blandford, R. D. 2007, ApJ, 667, 117
Tsuzuki, Y., Kawara, K., Yoshii, Y., Oyabu, S., Tanabé, T., & Matsuoka, Y. 2006, ApJ, 650, 57
Vanden Berk, D. E., et al. 2001, AJ, 122, 549
van der Marel, R. P., & Franx, M. 1993, ApJ, 407, 525
Vestergaard, M., & Wilkes, B. J. 2001, ApJS, 134, 1
Vestergaard, M. 2002, ApJ, 571, 733
Vestergaard, M., & Peterson, B. M. 2006, ApJ, 641, 689
Wandel, A., Peterson, B. M., & Malkan, M. A. 1999, ApJ, 526, 579
Wang, T.-G., Dong, X.-B., Zhang, X.-G., Zhou, H.-Y., Wang, J.-X., & Lu, Y.-J. 2005, ApJ, 625, L35
Wills, B. J., Netzer, H., Brotherton, M. S., Han, M., Wills, D., Baldwin, J. A., Ferland, G. J., & Browne, I. W. A. 1993, ApJ, 410, 534
Wu, S.-M., Wang, T.-G., & Dong, X.-B. 2008, MNRAS, 389, 213
York, D. G., et al. 2000, AJ, 120, 1579

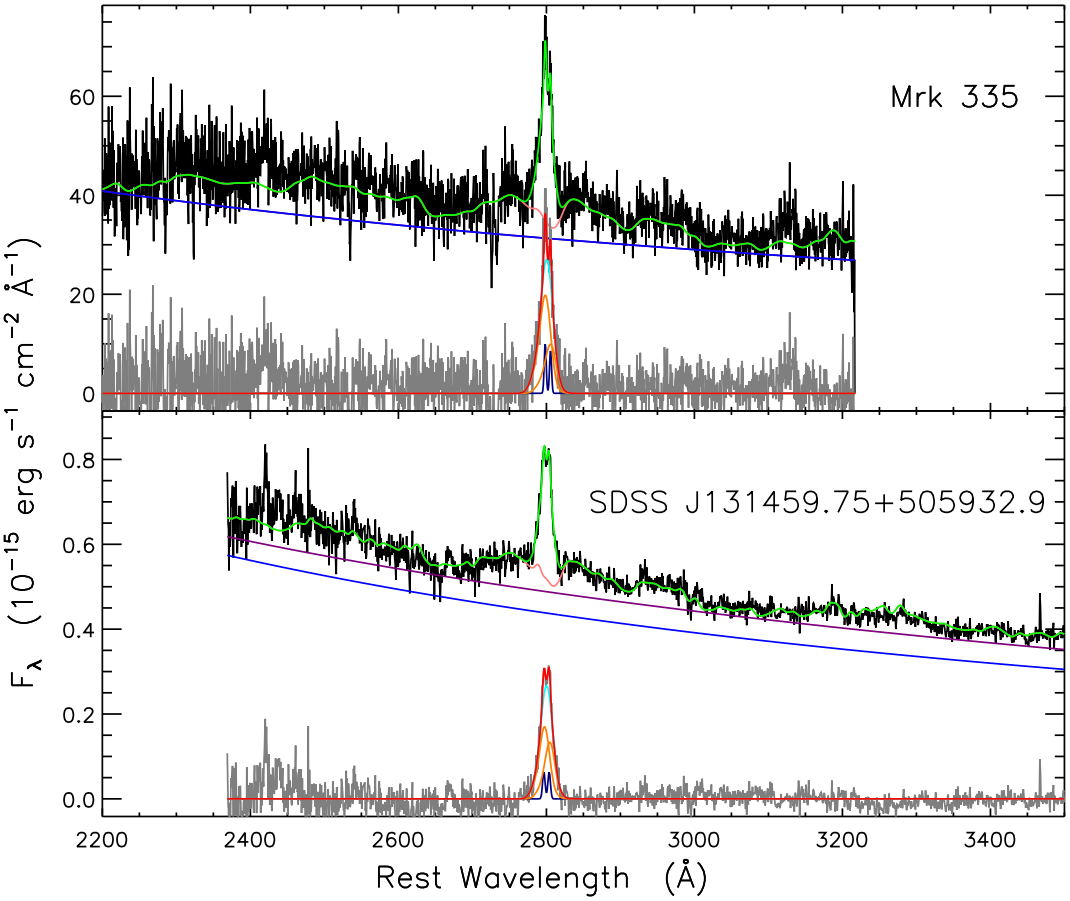

FIG. 1.— Examples of Mg II fitting for (*top*) the *HST* spectrum of Mrk 335 and (*bottom*) the SDSS spectrum of SDSS J131459.75+505932.9. The data are shown in black, the power-law AGN continuum in blue, the pseudocontinuum (power law plus Fe II emission) in pink, the final model for all fitted components in green, and the continuum-subtracted emission-line spectrum in gray. For the multi-Gaussian fit to Mg II, the narrow components are shown in navy, the individual broad components in brown, the sum of all the broad components in cyan, and the total model (narrow plus broad) in red.

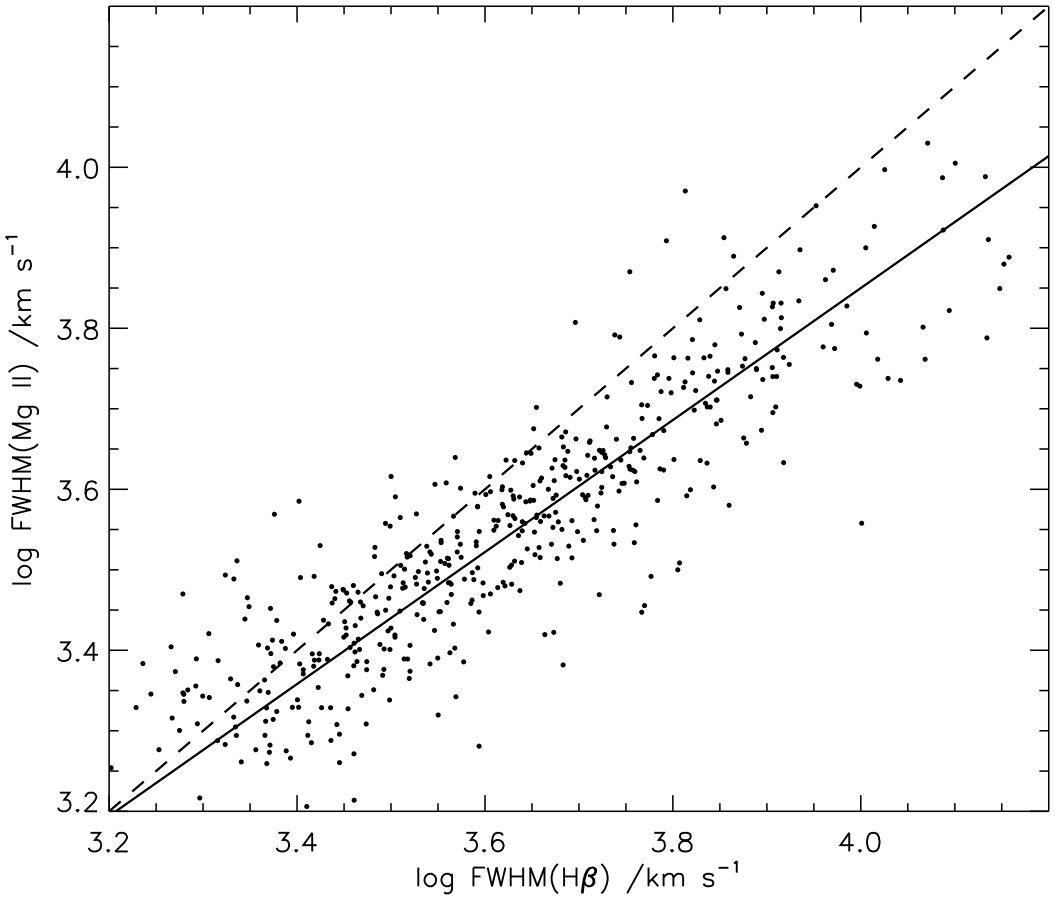

FIG. 2.— FWHM(Mg II) vs. FWHM(Hβ) for our SDSS sample. The solid line represents the best-fitting power law with index 0.81. The dashed line represents a 1:1 relationship.

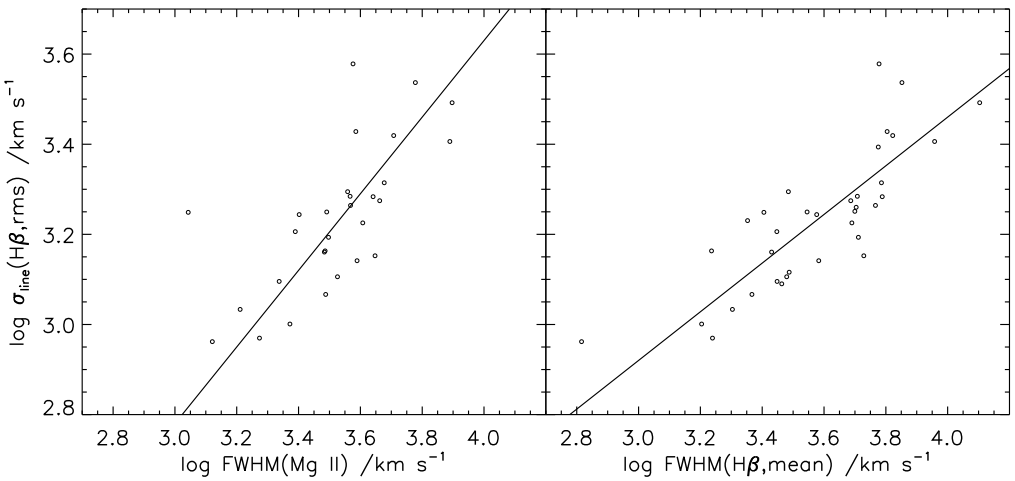

FIG. 3.— $\sigma_{\rm line}$(Hβ, rms) vs. (*left*) FWHM(Mg II) and (*right*) FWHM(Hβ, mean). The solid lines show the best-fitting relations.

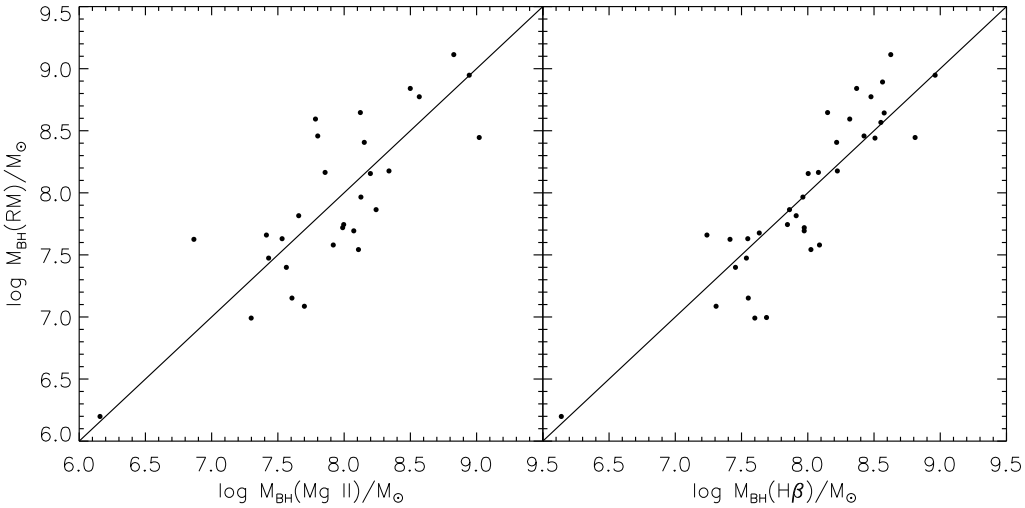

FIG. 4.— BH masses estimated from reverberation mapping plotted against masses obtained from (*left*) Mg II and (*right*) Hβ. The solid line represents a 1:1 relationship.

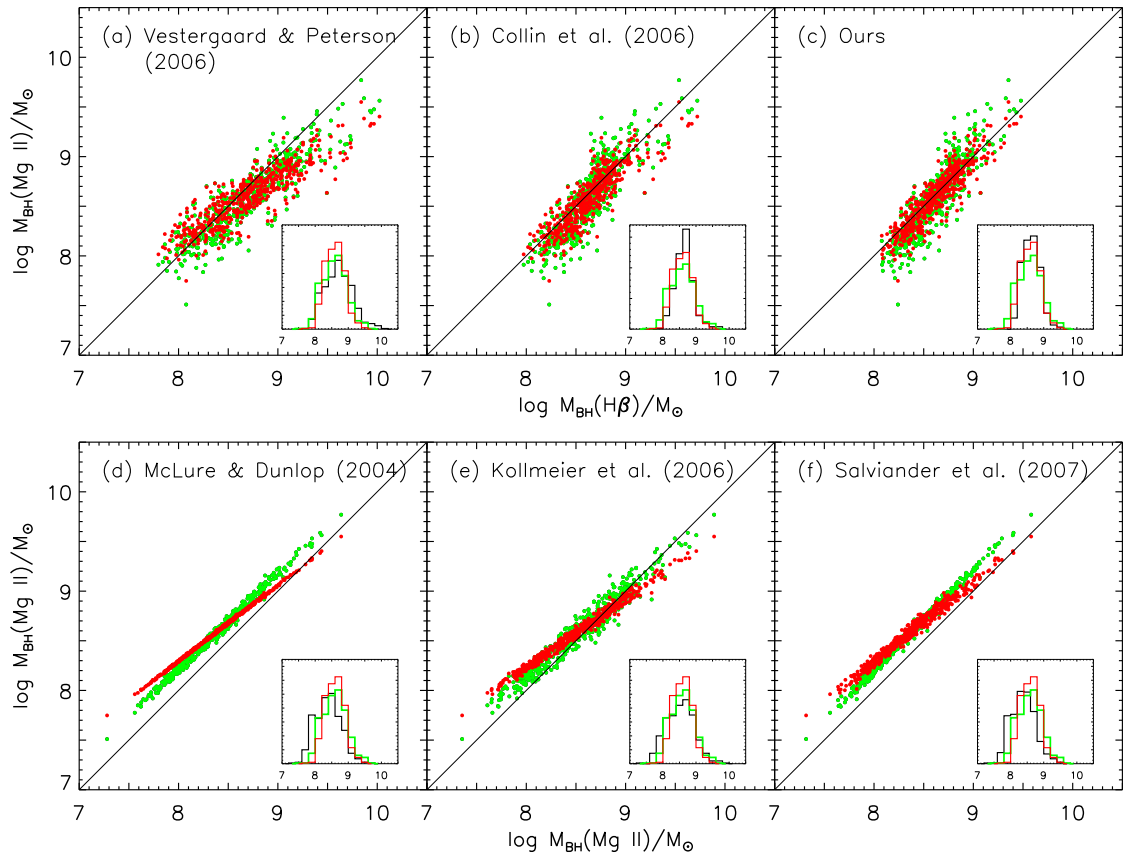

FIG. 5.— Comparison of $M_{\rm BH}$ estimated by our Mg II formalism with other formulae discussed in Section 3. The y-coordinates of the green and red points represent Mg II masses estimated by Scheme 2 ($M_{\rm BH} \propto {\rm FWHM}^2$) and Scheme 4 ($M_{\rm BH} \propto {\rm FWHM}^{1.51\pm0.49}$), respectively. The inset in each panel plots the histograms of $M_{\rm BH}$; green and red lines denote the Mg II-based masses from our Schemes 2 and 4, and black lines are the comparison masses. The top three panels compare our Mg II masses with masses derived from different Hβ formalisms. The Hβ masses from Vestergaard & Peterson (2006; *a*) are systematically different from our Mg II masses, while those of Collin et al. (2006; *b*) are roughly consistent, and the best agreement comes from our newly derived formalism (Equation 9; *c*, red points). The bottom three panels compare our Mg II-based masses with previous Mg II-based formalisms: McLure & Dunlop (2004; *d*), Kollmeier et al. (2006; *e*), and Salviander et al. (2007; *f*). All show systematic deviations, mostly in the sense of giving lower masses than our formalism.

TABLE 1
DATA FOR THE REVERBERATION-MAPPED SAMPLE

Name	DataID	$\log L_{3000}$ (erg s^{-1})	$\overline{\log L_{3000}}$ (erg s^{-1})	FWHM(Mg II) (km s^{-1})	$\overline{\rm FWHM(Mg\,II)}$ (km s^{-1})	$\log M_{\rm BH}$(RM) ($M_\odot$)
(1)	(2)	(3)	(4)	(5)	(6)	(7)
3C 120	lwp04153	44.46± 0.04	44.23± 0.01	2780	3074	7.74
	lwp04500	44.37± 0.03		3837		
	lwp05610	44.35± 0.02		2568		
	lwp09048	44.41± 0.03		2638		
	lwp09461	44.20± 0.02		3411		
	lwp09850	44.22± 0.02		3399		
	lwp10407	44.29± 0.04		4083		
	lwp11524	44.28± 0.03		2828		
	lwp11946	44.27± 0.03		2786		
	lwp12536	44.36± 0.03		2412		
	lwr01317	43.86± 0.08		2874		
	lwr02983	43.73± 0.02		2759		
	lwr06849	44.12± 0.03		3997		
	lwr09102	44.34± 0.03		2875		
	lwr09778	43.93± 0.02		2735		
	lwr13786	44.30± 0.02		2758		
	lwr15618	44.25± 0.03		3040		
	lwr16609	44.17± 0.04		3053		
	lwr16874	44.39± 0.06		4431		
3C 390.3	y33y0204t	42.63± 0.17	42.63± 0.17	7884	7884	8.46
Akn 120	y29e0305t	44.48± 0.08	44.48± 0.08	4377	4377	8.18
Fairall 9	y0ya0104t	44.30± 0.08	44.30± 0.08	3769	3769	8.41
Mrk 79	lwr01320	43.81± 0.02	43.71± 0.02	5057	4597	7.72
	lwr06141	43.60± 0.02		4179		
Mrk 110	lwp12760	43.64± 0.08	43.73± 0.05	2216	2355	7.40
	lwp12761	43.82± 0.07		2504		
Mrk 279	lwp02522	44.03± 0.03	43.89± 0.01	4812	4441	7.54
	lwp10116	43.77± 0.02		3314		
	lwp15450	43.03± 0.04		5330		
	lwp15687	43.75± 0.02		3275		
	lwp19173	43.98± 0.04		3555		
	lwp19220	44.02± 0.03		3987		
	lwp19598	44.28± 0.05		3699		
	lwp19937	44.20± 0.04		4204		
	lwp20271	44.26± 0.05		4305		
	lwp20725	44.18± 0.03		5057		
	lwr03073	43.03± 0.10		3710		
	lwr10816	43.98± 0.04		8201		
	lwr11623	43.94± 0.02		6934		
	lwr15803	43.96± 0.03		4121		
Mrk 335	y29e0205t	44.12± 0.04	44.13± 0.03	1977	1878	7.15
	y29e0206t	44.13± 0.05		1783		
Mrk 509	y0ya0305t	44.55± 0.05	44.55± 0.05	3357	3357	8.16
Mrk 817	lwr11936	44.07± 0.03	44.05± 0.03	3597	4053	7.69
	lwr13704	44.03± 0.04		4565		
NGC 3227	o5kp01010	41.76± 0.04	41.76± 0.04	3688	3688	7.63
NGC 3516	y31r0105t	43.05± 0.02	43.06± 0.01	3919	3699	7.63
	y31r0206t	43.23± 0.02		3775		
	y31r0306t	43.19± 0.02		3796		
	y31r0406t	42.73± 0.02		3499		
	y31r0506t	43.08± 0.02		3527		
NGC 3783	o57b01010	43.39± 0.06	43.39± 0.06	2524	2524	7.47
NGC 4051	lwp11100	41.76± 0.02	41.68± 0.01	1574	1322	6.20
	lwp12092	41.70± 0.02		1387		
	lwp12092	41.68± 0.02		1503		
	lwp19265	41.58± 0.02		1305		
	lwp20497	41.53± 0.02		946		
	lwp23153	41.70± 0.02		918		
	lwp24347	41.81± 0.02		752		
	lwp27297	41.77± 0.02		1349		
	lwp27298	41.77± 0.02		1667		
	lwr01728	41.76± 0.02		2582		
NGC 4151	o42303070	43.04± 0.03	42.62± 0.02	4905	3849	7.66
	o59701040	42.20± 0.02		3020		
NGC 4593	lwp02731	42.82± 0.02	42.82± 0.01	4123	3140	6.99
	lwp05348	42.82± 0.02		3022		
	lwp05371	42.81± 0.02		3288		
	lwp05394	42.83± 0.02		2778		
	lwp05411	42.80± 0.02		3444		
	lwp05430	42.74± 0.02		3107		
	lwp06266	42.64± 0.02		3237		
	lwp06300	42.72± 0.02		3033		
	lwp12278	43.01± 0.02		2822		
	lwp12279	43.03± 0.02		5194		
	lwr07884	42.83± 0.02		2723		
	lwr09818	42.77± 0.02		1929		
	lwr10539	42.86± 0.02		2987		
	lwr10622	42.81± 0.02		3117		
	lwr16177	42.87± 0.02		3321		
NGC 5548	y0ya0205t	43.01± 0.03	43.01± 0.03	4756	4756	7.82
NGC 7469	y3b6010bt	43.67± 0.03	43.67± 0.03	3061	3061	7.09
PG 0026+129	y2jk0108t	45.18± 0.04	45.18± 0.04	1104	1104	8.59
PG 0804+761	lwr13645	45.14± 0.02	45.04± 0.06	5175	3621	8.84

TABLE 2
CONTINUUM AND EMISSION-LINE PARAMETERS OF THE SDSS SAMPLE

SDSS Name (1)	z (2)	$\log L_{5100}$ (3)	FWHM(Hβ^b) (4)	$\log F$(Hβ^b) (5)	$\log F$(Hβ^n) (6)	$\log L_{3000}$ (7)	FWHM(Mg II^b) (8)	$\log F$(Mg II^b) (9)	$\log F$(Mg II^n) (10)
J000011.96+000225.3	0.478	44.69	3037	−14.06	−15.85	45.01	2892	−13.97	−16.01
J000110.97−105247.5	0.529	44.98	6807	−13.91	−15.71	45.24	6188	−14.08	−15.25
J001725.36+141132.6	0.514	45.23	5676	−13.67	−15.70	45.56	4469	−13.84	−14.86
J002019.22−110609.2	0.492	44.85	2832	−13.91	···	45.09	2664	−14.08	−16.33
J005121.25+004521.5	0.727	45.04	2572	−14.32	−15.31	45.23	1624	−14.67	−15.66
J005441.19+000110.7	0.646	45.08	2220	−14.46	···	45.22	2101	−14.41	−15.43
J010448.57−091013.0	0.469	44.77	4610	−13.98	−15.49	44.97	2672	−14.26	−16.04
J010644.16−103410.6	0.468	44.72	3873	−13.99	−15.52	44.99	3228	−13.95	−15.46
J011132.34+133519.0	0.576	45.13	8060	−13.86	−15.92	45.46	5805	−14.01	−14.97
J012016.73−092028.8	0.495	44.71	3284	−13.89	−16.19	45.15	3334	−13.75	−16.23

NOTE. — Col. (1) Object name. Col. (2) Redshift derived from the peak of [O III] λ5007. Col. (3) Luminosity of the power-law continuum at 5100 Å. Col. (4) FWHM of broad Hβ. Col. (5) Flux of the broad component of Hβ. Col. (6) Flux of the narrow component of Hβ. Col. (7) Luminosity of the power-law continuum at 3000 Å. Col. (8) FWHM of broad Mg II. Col. (9) Flux of the broad component of Mg II. Col. (10) Flux of the narrow component of Mg II. Luminosities, fluxes, and FWHM are in units of erg s^{-1}, erg s^{-1} cm^{-2}, and km s^{-1}, respectively. *Table 2 is available in its entirety via the link to the machine-readable table above. A portion is shown here for guidance regarding its form and content.*

TABLE 3
REGRESSION RESULTS FOR

$$\log \frac{\rm FWHM(Mg\,II)}{1000\ {\rm km\ s^{-1}}} = k \log \frac{\rm FWHM(H\beta)}{1000\ {\rm km\ s^{-1}}} + c$$

Method	k	c
OLS	0.73 ± 0.02	0.09 ± 0.01
WLS	0.73 ± 0.02	0.09 ± 0.01
FITexy	0.77 ± 0.01	0.06 ± 0.02
FITexy_T02	0.81 ± 0.03	0.04 ± 0.02
Gaussfit	0.81 ± 0.03	0.04 ± 0.02
BCES(bisector)	0.78 ± 0.03	0.06 ± 0.02
BCES(orthogonal)	0.81 ± 0.02	0.05 ± 0.01
LINMIX_ERR	0.81 ± 0.03	0.04 ± 0.02

TABLE 4
REGRESSION RESULTS FOR $\log\left[\frac{M_{\rm BH}({\rm RM})}{10^6\,M_\odot}\right] = a + \beta \log \frac{L_{3000}}{10^{44}\ {\rm erg\ s^{-1}}} + \gamma \log\left[\frac{\rm FWHM(Mg\,II)}{1000\ {\rm km\ s^{-1}}}\right]$ AND $M_{\rm BH}$ COMPARISONS

Scheme	a	β	γ	$\Delta M_{\rm BH}$(RM)	$\Delta M_{\rm BH}(\rm H\beta)$ (Vestergaard & Peterson 2006)	$\Delta M_{\rm BH}(\rm H\beta)$ (Collin et al. 2006)	$\Delta M_{\rm BH}(\rm H\beta)$ (Ours)
(1)	(2)	(3)	(4)	(5)	(6)	(7)	(8)
Scheme 1[a]	1.15 ± 0.27	0.46 ± 0.08	1.48 ± 0.49	0.00 ± 0.39	0.15 ± 0.22	0.10 ± 0.14	0.07 ± 0.12
Scheme 2	0.88 ± 0.08	0.48 ± 0.08	2	0.00 ± 0.42	0.11 ± 0.19	0.06 ± 0.18	0.03 ± 0.18
Scheme 3	1.03 ± 0.08	0.48 ± 0.08	1.70	0.00 ± 0.40	0.13 ± 0.20	0.07 ± 0.15	0.05 ± 0.14
Scheme 4	1.13 ± 0.27	0.5	1.51 ± 0.49	0.00 ± 0.40	0.10 ± 0.21	0.05 ± 0.14	0.03 ± 0.12

NOTE. — $\Delta M_{\rm BH} \equiv \log M_{\rm BH} - \log M_{\rm BH}({\rm Mg\,II})$ are the residuals of the masses estimated by our Mg II formalism with masses obtained from reverberation mapping (Col. 5), Hβ according to the formalism of Vestergaard & Peterson (2006; Col. 6), Hβ according to the formalism of Collin et al. (2006; Col. 7), and Hβ according to our formalism for the SDSS sample (Equation 9; Col. 8).

[a]Scheme 1 was fitted using the code MLINMIX_ERR of Kelly (2007).